applied sciences

MDPI

Article

Experimental Study on the Effect of Leading-Edge Curvature Optimization on Pressure Fluctuations in Transonic Compressor Blades

Ye Yang [1], Shaozun Hong [1], Yuan Yi [1], Xingya Da [1] and Junqiang Wu [2,*]

[1] High Speed Aerodynamics Institute, China Aerodynamics Research and Development Center, Mianyang 621000, China
[2] China Aerodynamics Research and Development Center, Mianyang 621000, China
* Correspondence: wujunqiang_cardc@163.com

Abstract

To investigate the impact of continuous leading-edge curvature on the aerodynamic performance of transonic compressor blade profiles, schlieren observations and surface pulsating pressure measurements were conducted on the baseline profile CM1.2 and its optimized variant CM1.2-Y. The results indicate that the optimized profile can effectively reduce unsteady pressure pulsations at Mach numbers of 0.8 and 1.05, with a maximum reduction of 14.6 dB. At Mach number 0.95, the optimized design eliminates high-pressure pulsation regions on the pressure surface but intensifies local loading on the suction surface. The optimization of leading-edge curvature effectively reduces the extreme pulsations on the suction surface caused by shock wave interference under most operating conditions, and significantly improves the wave structure on the pressure surface, thereby comprehensively reducing the pressure pulsation level of the blade profile.

Keywords: transonic compressor; blade leading edge; curvature continuity; pressure fluctuation; schlieren

1. Introduction

The aerodynamic performance of modern aero-engines directly determines the comprehensive performance of aircrafts. As the core component, the compressor undertakes the crucial task of compressing and pressurizing the incoming airflow [1]. With the development of aviation technology, transonic compressors have become an important choice for advanced aero-engines due to their ability to achieve higher pressure ratios and efficiencies in a single stage [2]. However, the complex flow phenomena under transonic conditions pose severe challenges to the compressor design: when the airflow velocity approaches or exceeds the speed of sound, unsteady flow phenomena such as shock waves, shock wave–boundary layer interactions, and flow separation occur on the blade surface. These phenomena not only lead to significant energy losses but also induce strong unsteady pressure fluctuations [3].

Unsteady pressure fluctuations are a crucial feature of internal flow in transonic compressors, and their generation mechanism involves various physical processes such as shock wave oscillations and separation bubble pulsations [4]. Intense pressure fluctuations can induce blade vibrations and aerodynamic noise, potentially leading to high-cycle fatigue failure of the blades in severe cases [5]. Therefore, a deep understanding of the unsteady pressure fluctuation characteristics on the blade surface of transonic compressors and the

Academic Editors: Izabela Krzysztofik, Grzegorz Kopecki, Slawomir Blasiak and Andrzej Żyluk

Received: 7 April 2026
Revised: 12 May 2026
Accepted: 12 May 2026
Published: 13 May 2026

exploration of effective flow control methods hold significant theoretical and engineering value for enhancing the aerodynamic performance of compressors [6]. Among the numerous geometric parameters that affect the aerodynamic performance of transonic compressor blades, the distribution of leading-edge curvature directly influences the position, intensity, and morphology of shock waves [7]. However, current research on the impact of leading-edge curvature optimization on unsteady pressure fluctuations in transonic compressor blades remains insufficiently systematic, particularly regarding the influence patterns under different Mach numbers and angles of attack. This uncertainty constrains the refined design of high-performance compressor blades [8].

Scholars both domestically and internationally have conducted extensive research on the relationship between the leading-edge shape and aerodynamic performance of transonic compressor airfoils. In the early days, Lee [1] was the first to propose the trailing-edge feedback mechanism of supersonic airfoil shock wave oscillation, laying the foundation for understanding transonic unsteady flows. Denton [9] systematically summarized the loss mechanisms in turbomachinery, pointing out that shock wave losses and suction surface boundary layer losses dominated in transonic compressors, and the leading-edge geometry directly determined the level of loss by affecting the position and intensity of the shock wave. Hilgenfeld [10] experimentally studied the turbulence structure in high-load transonic compressor cascades, revealing the complexity of shock wave/laminar boundary layer interactions. Based on this, Du et al. [11] established a shock wave loss model for transonic axial compressors, and Yang [12] discovered the phase lag effect in unsteady flows through three-dimensional oscillating cascade experiments, providing an important reference for subsequent research on unsteady pressure pulsations.

In terms of leading-edge geometry optimization, Goodhand [13] proposed a new performance criterion for the "spike" phenomenon at the compressor leading edge, quantifying the impact of leading-edge velocity spike intensity on boundary layer stability; Meng [6] introduced a new blade profile parameterization method, which reduced the total pressure loss coefficient of transonic compressor cascades by 11% by optimizing the leading-edge curvature distribution; Shi Hengtao [14] proposed a curvature-continuous leading-edge modeling method based on polynomials, expanding the operating range by 3.1° to 3.8°; Khan [15] used the high-pressure transonic centrifugal compressor SRV2 developed by the German Aerospace Center as the object, parameterized the blade shape using Bezier curves, and studied the effect of an optimized blade profile on compressor performance through a numerical simulation. This study verified the feasibility of improving the stable working range of the compressor through a numerical simulation combined with profile parameterization optimization, and provided an important reference for optimizing the leading-edge curvature of transonic blades. Liu Jisheng [16] optimized the ellipticity of the transonic blade profile leading edge, identifying the optimal ellipticity range as [0.8, 0.9]; Zou [7] studied the synergistic improvement in leading-edge contour accuracy and aerodynamic performance in robotic grinding; Li [8] redesigned the leading-edge contour based on B-spline curves, achieving a continuous curvature distribution; Chen [17] combined reinforcement learning with aerodynamic optimization, finding that reducing the leading edge could effectively suppress transonic buffeting; Wang [18] investigated the impact of flexible trailing edge deformation methods on the aerodynamic performance of transonic airfoils; Liu [19] proposed an aerodynamic optimization platform based on radial basis functions, improving the adiabatic efficiency of NASA Rotor 37 by 1.47%. These studies mainly focus on improving steady-state aerodynamic performance, providing a theoretical basis for leading-edge curvature optimization.

However, the inherently unsteady nature of transonic flows necessitates researchers to focus on the mechanism of dynamic pressure fluctuations. Giannelis [20] provided a

systematic review of the mechanism of transonic shock wave buffeting; Munoz Lopez [21] uncovered the physical mechanism of shock wave oscillation through time-resolved particle image velocimetry (PIV) measurements, pointing out that the periodic expansion and contraction of the separation bubble were the primary drivers of pressure fluctuations; Wang [22] investigated the characteristics of shock wave/boundary layer interactions using large-eddy simulation; Meng [23] studied shock wave–boundary layer interactions in high-load transonic compressor cascades through experimental and numerical methods; Watanabe [24] achieved a high-frequency measurement of unsteady pressure on oscillating blade surfaces using fast-response pressure sensitive paint (PSP) technology; Malzacher [25] conducted systematic experiments on aerodynamically mistuned oscillating compressor cascades and discovered modal coupling effects; Gan [26] investigated the influence of shock wave behavior on the unsteady aerodynamic characteristics of oscillating transonic compressor cascades and found a close correlation between the oscillation frequency of the shock wave and the blade vibration frequency. These studies have deepened our understanding of unsteady flow mechanisms, but they mostly focus on shock wave oscillation itself, and there is still a lack of research on how the optimization of leading-edge curvature quantitatively affects the intensity of pressure fluctuations.

Based on the above research status, it can be observed that existing studies primarily focus on the influence of leading-edge shape on the steady-state aerodynamic performance of transonic compressor blade profiles (such as total pressure loss, efficiency, operating range, etc.). However, there is still a significant gap in research regarding the impact of leading-edge curvature optimization on the unsteady pressure fluctuation characteristics of the blade surface. On the one hand, existing studies often concentrate on steady-state performance parameters, with a relative lack of exploration into unsteady pressure fluctuations, a crucial flow characteristic. On the other hand, the existing research primarily employs numerical simulation methods, lacking systematic experimental verification, making it difficult to accurately capture complex unsteady flow phenomena induced by shock wave–boundary layer interactions. Therefore, this article takes the CM1.2 blade profile as the research object, and continuously optimizes the curvature of its leading edge. The experimental method combining schlieren measurement and surface pulsating pressure measurement is used to study the influence of leading-edge curvature optimization on the flow field schlieren image, pulsating pressure sound pressure level, and pulsating pressure spectrum characteristics of the blade profile under different Mach numbers and angles of attack.

2. Methods

2.1. Experimental Equipment and Testing Methods

The experiment was conducted in the 0.6 m × 0.6 m transonic–supersonic wind tunnel of the China Aerodynamics Research and Development Center. The Mach number range of this wind tunnel is 0.4 to 2.5, and the Reynolds number range is (8 to 33) × 10^6 m^{-1}. The cross-sectional dimensions of the test section of the wind tunnel are 0.6 m × 0.6 m, and the length of the test section is 1.775 m. The performance indicators of Mach number, flow field uniformity, turbulence intensity, etc., in the experimental section all comply with GJB1179-91 [27]. By conducting fluctuating pressure measurements and schlieren measurements, the fluctuating pressure characteristics and flow characteristics on the model surface were obtained.

2.2. Experimental Models

The test models are CM1.2 and CM1.2-Y, where CM1.2 serves as the baseline airfoil and CM1.2-Y represents the airfoil with optimized leading-edge curvature. The CST (class

function/shape function transformation) method [28] was used to modify the reference blade profile. Firstly, the CST method was used to fit the reference blade profile, and then the class function coefficients of the leading edge were modified to change the shape of the leading edge, generating a new curvature-continuous blade profile. When the class function coefficient of the current edge is 0.7, the CM1.2-Y leaf shape can be obtained. The leading-edge radius of CM1.2 airfoil is 1.97 mm. A comparison of the leading edges of the CM1.2 and CM1.2-Y airfoils is illustrated in Figure 1. Taking into account factors such as leading-edge machining accuracy, wind tunnel blockage, and sensor installation, the airfoil model has a chord length of 525 mm and a span length of 370 mm. The installation of the airfoil model in the wind tunnel is depicted in Figure 2. In the wind tunnel, the blockage at the model's zero angle of attack is 4.2%. Pulsating pressure sensors are arranged on the surface of the airfoil model, with a measuring point aperture of 1.7 mm. The locations of the measuring points are shown in Figure 3. Twelve pulsating pressure measuring points are arranged on each of the upper and lower surfaces of the airfoil model, for a total of 24 measuring points. The midpoint of the chord line is taken as the origin, with the positive x-direction extending from the leading edge to the trailing edge. The locations of each measuring point are detailed in Table 1.

Table 1. Location of pulsating pressure measuring point.

Measuring Point Number	Position/mm
1	−150
2	−100
3	−75
4	−50
5	−25
6	0
7	25
8	50
9	75
10	100
11	125
12	150
13	−150
14	−100
15	−75
16	−50
17	−25
18	0
19	25
20	50
21	75
22	100
23	125
24	150

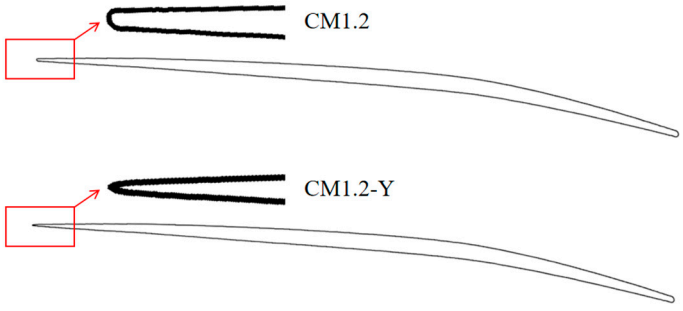

Figure 1. Comparison of leading edges between CM1.2 blade profile and CM1.2-Y blade profile.

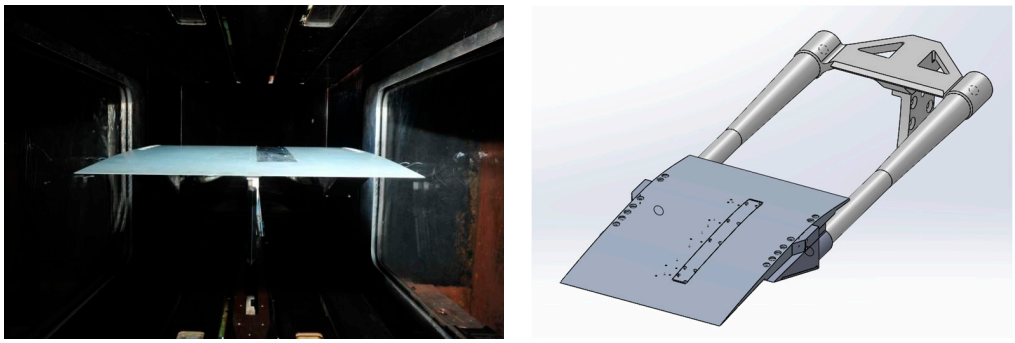

(a) Photos of the model in the wind tunnel (b) Schematic diagram of experimental device structure

Figure 2. Test device.

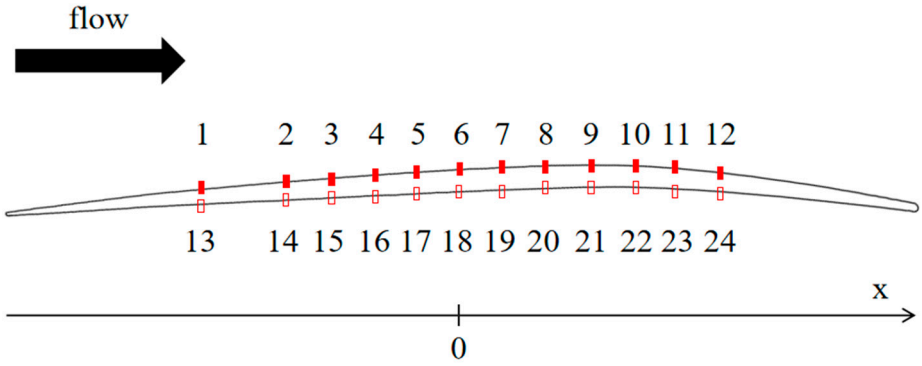

Figure 3. Schematic diagram of measuring point locations.

2.3. Test Instrument

The optical path of the schlieren system adopts a "Z"—shaped layout, with a green LED (521–535 nm) light source, an effective light diameter of 250 mm, an effective pixel count of 8.8 million for the camera, and a frame rate of 30 fps. The pulsating pressure sensor is a piezoresistive type with a measurement range of 206 kPa and a natural frequency of 200 kHz. The data acquisition and analysis processing system utilizes the DEWEsoft (X2 SP6 version) system, with a sampling frequency of 50 kHz and a sampling duration of 10 s during the test.

2.4. Data Processing Method

The total sound pressure level of pulsating pressure is calculated using Formulas (1) and (2).

Root mean square value of pulsating pressure

$$P_{rms} = \lim_{T\to\infty}\sqrt{\frac{1}{T}\int_0^T p^2(t)dt} \quad (1)$$

Pulsating pressure sound pressure level

$$SPL = 20\lg\left(\frac{P_{rms}}{P_{ref}}\right) \quad (2)$$

Among them, reference pressure $P_{ref} = 2 \times 10^{-5}$ Pa.

The sound pressure spectrum can be calculated using the following formula: first, perform a fast Fourier transform (FFT) on the measured pulsating pressure values, and then calculate and process according to Formula (3),

Power spectral density function

$$P(f) = \lim_{\Delta f \to 0} \frac{1}{\Delta f} \left[\lim_{T \to \infty} \frac{1}{T} \int_0^T p^2(t, f, \Delta f) dt \right] \quad (3)$$

Sound pressure spectrum

$$SPFS = 10\lg \frac{P(f)}{P_{\text{ref}}^2} \quad (4)$$

3. Results and Discussion

To systematically evaluate the impact of leading-edge curvature optimization on the flow field structure and surface pulsating pressure characteristics of compressor airfoils, this study conducted schlieren tests and surface pulsating pressure measurement tests on the baseline CM1.2 airfoil and its optimized variant CM1.2-Y at Mach numbers of 0.8, 0.95, and 1.05 under multiple angles of attack. Due to the size limitation of the schlieren window, only the local area of the airfoil's leading edge was observed.

3.1. Surface Flow Characteristics

The analysis of schlieren images in this article is mainly qualitative analysis, aiming to provide a visual understanding of the pulsating pressure characteristics on the blade surface in Section 3.2. The schlieren image reflects the density gradient. According to equation of state (5), it can be approximated that pressure and density are proportional when the temperature change is not significant. All the schlieren results in this article can be approximated as indicating that the pressure gradient and density gradient of the airflow change synchronously.

$$P = \rho \mathrm{RT} \quad (5)$$

3.1.1. Ma = 0.8

The schlieren test results of the CM1.2 blade profile, Mach number 0.8, and angle of attack range -3° to $+3^\circ$ are shown in Figure 4a–g. In Figure 4a, at an angle of attack of -3°, when the airflow passes near the leading edge, there is a large elliptical expansion area on the lower side of the model with a large density gradient. After expansion acceleration, a normal shock wave perpendicular to the wall appeared and the airflow passed through the shock wave, resulting in a significant decrease in density gradient and pressure gradient.

As the angle of attack increases, as shown in Figure 4b–d, the elliptical expansion region near the leading edge becomes smaller, indicating that the airflow density and pressure changes tend to be smoother. As the angle of attack further increases, as shown in Figure 4e–g, the elliptical region near the leading edge gradually decreases, and the shock wave region disappears, indicating that the density gradient and pressure gradient further decrease. Based on the above results, it can be concluded that the position and shape of the shock wave are sensitive to changes in the angle of attack. At negative angles of attack (-3° to -1°), the shock wave is located below the leading edge and its intensity decreases as the angle of attack increases. At positive angles of attack ($+1^\circ$ to $+3^\circ$), the shock wave near the leading edge disappears, and the density gradient near the leading edge decreases as the angle of attack increases. In all tested ranges of angles of attack, the pressure gradient in the local region near the leading edge decreases as the angle of attack increases.

To evaluate the improvement effect of leading edge curvature optimization on the aerodynamic performance of the airfoil at Mach number 0.8, the same schlieren comparison experiment was conducted on the optimized airfoil CM1.2-Y as on the baseline CM1.2 airfoil, with an angle of attack ranging from $\alpha = -3^\circ$ to $+3^\circ$, covering a total of seven operating conditions. Comparing Figures 4a and 5a, it can be seen that at the same Mach

number and angle of attack (−3°), and only by changing the leading-edge curvature, the elliptical expansion region of the leading edge of the airfoil in Figure 5a is significantly reduced, indicating a decrease in density gradient and pressure gradient. Similar situations are observed in Figure 5b–g, indicating that under the same operating conditions, compared to the baseline airfoil, the optimized leading edge curvature of CM1.2-Y results in smaller density and pressure gradients near the leading edge. Based on the above results, it is concluded that at Mach number 0.8, compared to the baseline airfoil, the leading-edge curvature optimization of CM1.2-Y effectively reduces pressure non-uniformity, thereby improving the uniformity and stability of the leading-edge flow field.

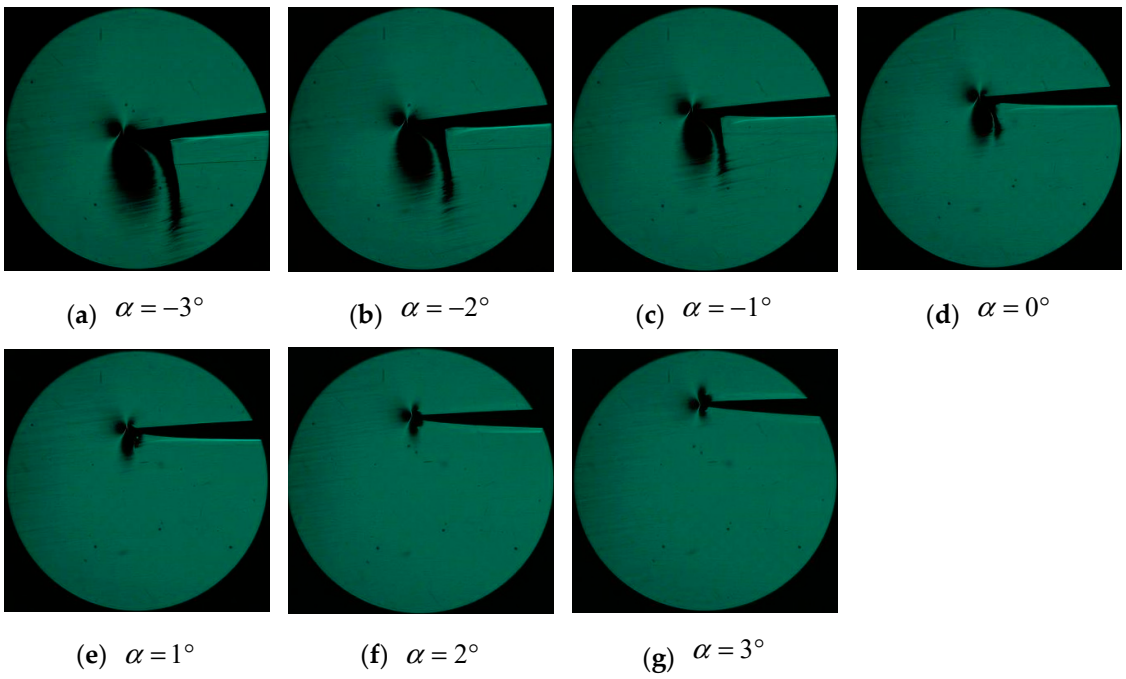

Figure 4. Schlieren image of CM1.2 blade profile at Mach number 0.8.

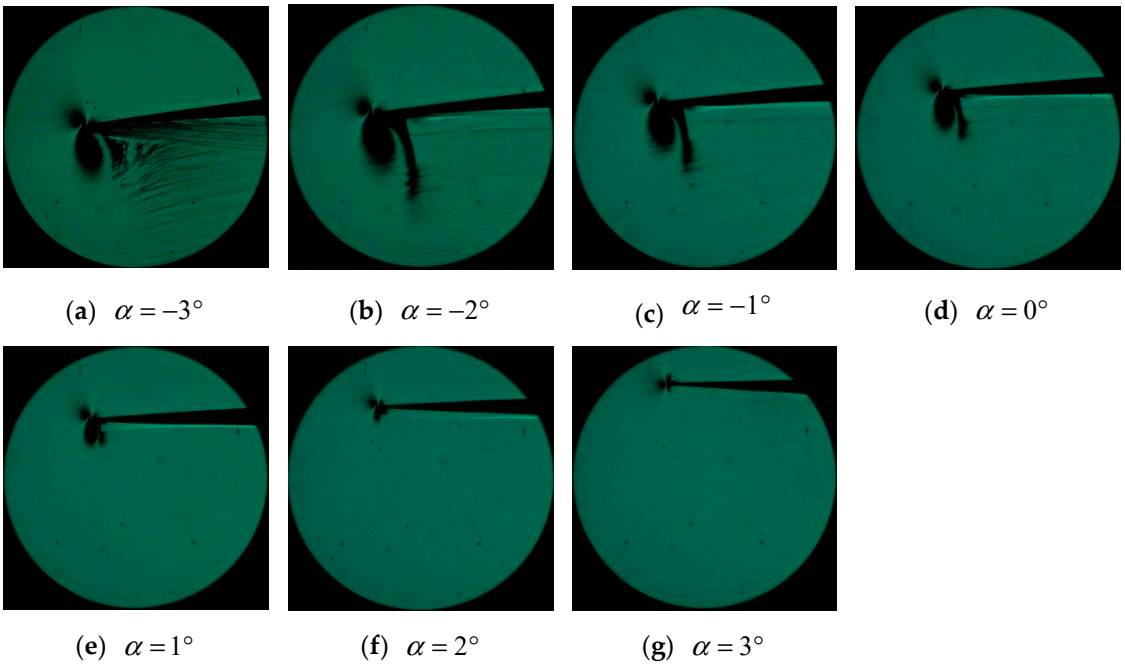

Figure 5. CM1.2-Y blade profile, Mach number 0.8 schlieren image.

3.1.2. Ma = 0.95

The schlieren test results for the CM1.2 airfoil at a Mach number of 0.95 and an angle of attack ranging from −3° to +3° are shown in Figure 6a–g. As can be seen from Figure 6a (angle of attack of −3°), compared to the case at a Mach number of 0.8 (Figure 4a), a strong oblique shock wave appears below the leading edge of the airfoil at a Mach number of 0.95, with a larger shock wave angle. From Figure 6a (angle of attack of −3°) to Figure 6d (angle of attack of 0°), it can be observed that as the angle of attack increases, the shock wave angle also increases. A normal shock wave appears downstream of the oblique shock wave, indicating that the airflow line decelerates and pressurizes through the oblique shock wave, then accelerates to supersonic speed through the expansion wave region, and finally decelerates and pressurizes again through the normal shock wave. Compared to the case at a Mach number of 0.8 (Figure 4a–g), a shadow area appears above the leading edge of the airfoil in Figure 6a–g, indicating that as the Mach number increases, the changes in density gradient and pressure gradient become more pronounced. Based on the above results, it is concluded that under the condition of a Mach number of 0.95, the leading-edge flow field of the CM1.2 airfoil exhibits characteristics of increased shock wave intensity and generally increased pressure gradient.

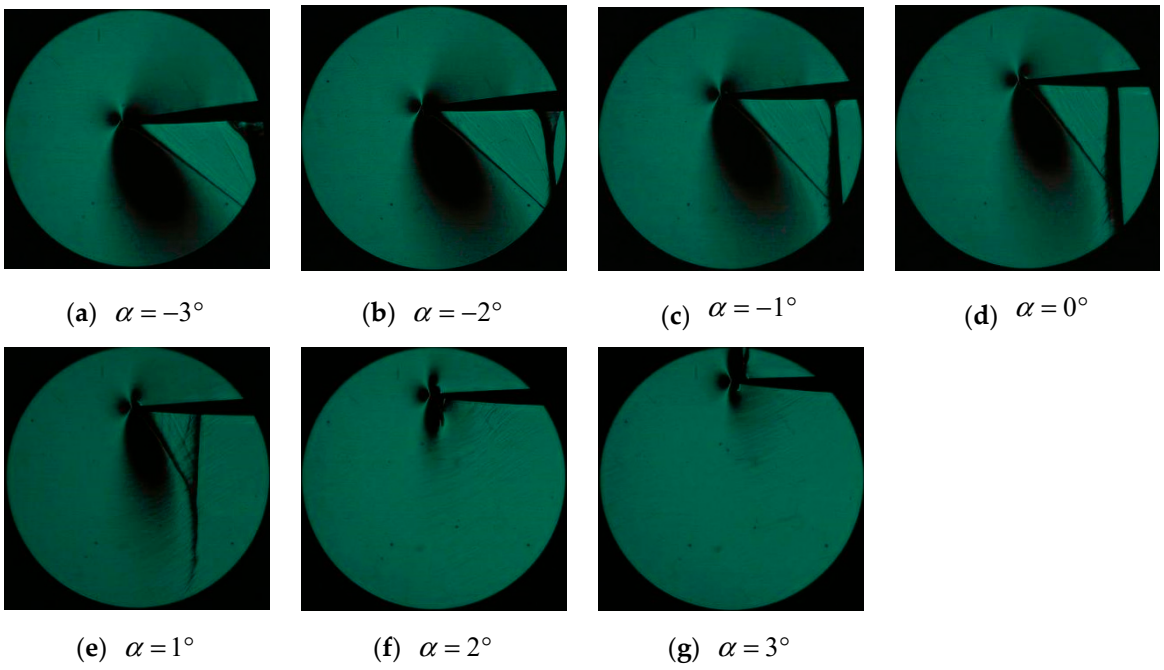

Figure 6. CM1.2 blade profile, Mach number 0.95 schlieren image.

The schlieren test results for the CM1.2-Y airfoil at a Mach number of 0.95 and an angle of attack ranging from −3° to +3° are shown in Figure 7a–g. In Figure 7a (angle of attack of −3°), an oblique shock wave is present below the leading edge. However, compared to the baseline CM1.2 airfoil (Figure 6a), the leading-edge oblique shock wave changes from a sharp thin line to a thicker line with a certain thickness, indicating a decrease in shock wave intensity. Moreover, compared to the baseline airfoil, the shock wave angle decreases, making it closer to the leading-edge surface. The normal shock wave that appears slightly behind the leading edge of the airfoil has an increased width in the shadowed area compared to the baseline airfoil, indicating a reduced density gradient and decreased shock wave intensity. Since gas pressure is proportional to density, this also indicates a decreasing pressure gradient, proving that after optimizing the leading-edge curvature, the pressure change on the lower surface of the model becomes smoother. In

Figure 7b–d (angles of attack of −2°, −1°, 0°, 1°), similar to the case at an angle of attack of −3°, the leading-edge oblique shock wave changes from a thin line to a thicker line, indicating a decrease in shock wave intensity. The position of the normal shock wave on the lower side of the airfoil moves towards the leading edge, and the dark shadow of the normal shock wave widens, indicating a smoother density transition before and after the shock wave. In Figure 7f (angle of attack of 2°), compared to the baseline CM1.2 airfoil, a normal shock wave appears behind the leading edge, indicating an increased pressure gradient. In Figure 7g, compared to the baseline CM1.2 airfoil (Figure 6g), the area of the shadowed region near the leading edge significantly decreases, indicating a more uniform density gradient and smoother pressure change.

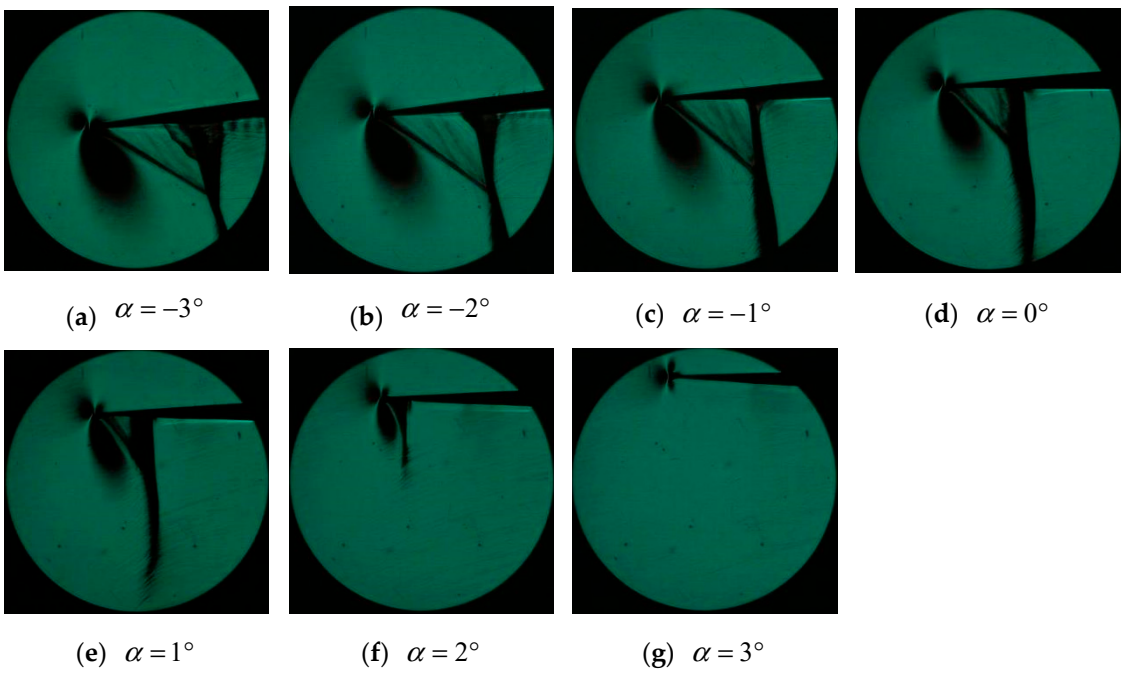

Figure 7. CM1.2-Y blade profile, Mach number 0.95 schlieren image.

Based on the above results, it can be concluded that under the condition of Mach number 0.95, compared to the baseline CM1.2 airfoil, the optimized airfoil significantly improves the flow field at most tested angles of attack. The intensity of the oblique shock wave at the leading edge decreases, as does the intensity of the normal shock wave on the lower surface of the model. Overall, the pressure gradient near the leading edge decreases, and the pressure variation becomes more gradual. However, the position of the normal shock wave moves towards the leading edge, which may lead to an increase in pulsating pressure at some locations.

3.1.3. Ma = 1.05

The schlieren test results for the CM1.2 airfoil at a Mach number of 1.05 and an angle of attack ranging from −3° to +3° are shown in Figure 8a–g. In Figure 8a, at a Mach number of 1.05 and an angle of attack of −3°, an oblique shock wave appears on the lower side of the airfoil's leading edge. Compared to the condition at a Mach number of 0.95 and an angle of attack of −3° (Figure 6a), the normal shock wave closer to the downstream is positioned further back and does not appear within the schlieren viewing window. The patterns for angles of attack ranging from −2° to 1° (Figure 8b–e) are similar to that of −3° (Figure 8a). Compared to the condition at a Mach number of 0.95 and angles of attack ranging from −2° to 1° (Figure 6b–e), the downstream normal shock wave is positioned further back and does not appear within the schlieren viewing window. Furthermore, as

the Mach number increases, the shadow area of the elliptical expansion region near the leading edge becomes larger, indicating greater density and pressure gradients. In Figure 8f (Mach number 1.05, angle of attack of 2°), compared to Figure 6f (Mach number 0.95, angle of attack of 2°), not only is the shadow area near the leading edge larger, but there is also an oblique shock wave. In Figure 8g (Mach number 1.05, angle of attack of 3°), compared to Figure 6g (Mach number 0.95, angle of attack of 3°), the shadow area on the upper side of the airfoil's leading edge is larger. Based on these results, it can be concluded that under the condition of a Mach number of 1.05, the reference CM1.2 airfoil exhibits a larger area of density gradient variation, stronger pressure gradient variation, and a more posterior position of the normal shock wave.

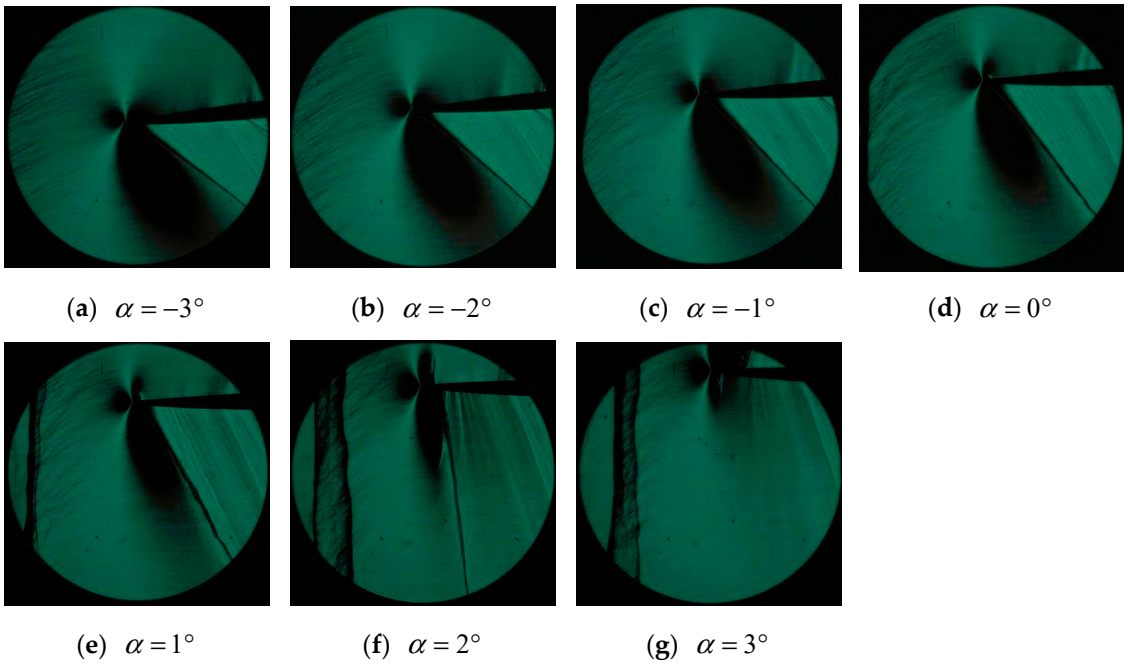

Figure 8. CM1.2 blade profile, Mach number 1.05 schlieren image.

The schlieren test results for the CM1.2-Y blade profile at a Mach number of 1.05 and an angle of attack ranging from −3° to +3° are shown in Figure 9a–g. In Figure 9a, it can be observed that under the condition of Mach number 1.05 and an angle of attack of −3°, after optimizing the blade profile leading edge, compared to the baseline blade profile (Figure 8a), the elliptical expansion wave region in front of the leading edge is smaller, the schlieren light–dark transition zone is wider, the density variation in this region on the surface is smoother, and the pressure peak after the expansion wave region is reduced; moreover, the subsequent oblique shock wave width is longer, the intensity of the oblique shock wave on the surface decreases, and the pressure gradient variation becomes smoother. In Figure 9b–d, the conditions at angles of attack ranging from −2° to 0° are similar to those at an angle of attack of −3°. Compared to the baseline blade profile, the expansion wave region of the leading edge optimized blade profile is smaller, the shock wave intensity is lower, and the pressure variation is smoother. In Figure 9e, compared to the baseline blade profile (Figure 8e), the oblique shock wave behind the leading edge is significantly weakened. In Figure 9f, the expansion wave region near the leading edge is significantly reduced, indicating a smoother pressure variation, but the normal shock wave moves forward towards the leading edge, indicating pressure fluctuations behind the leading edge. In Figure 9g, compared to the baseline blade profile (Figure 8g), the expansion wave region at the leading edge is significantly reduced.

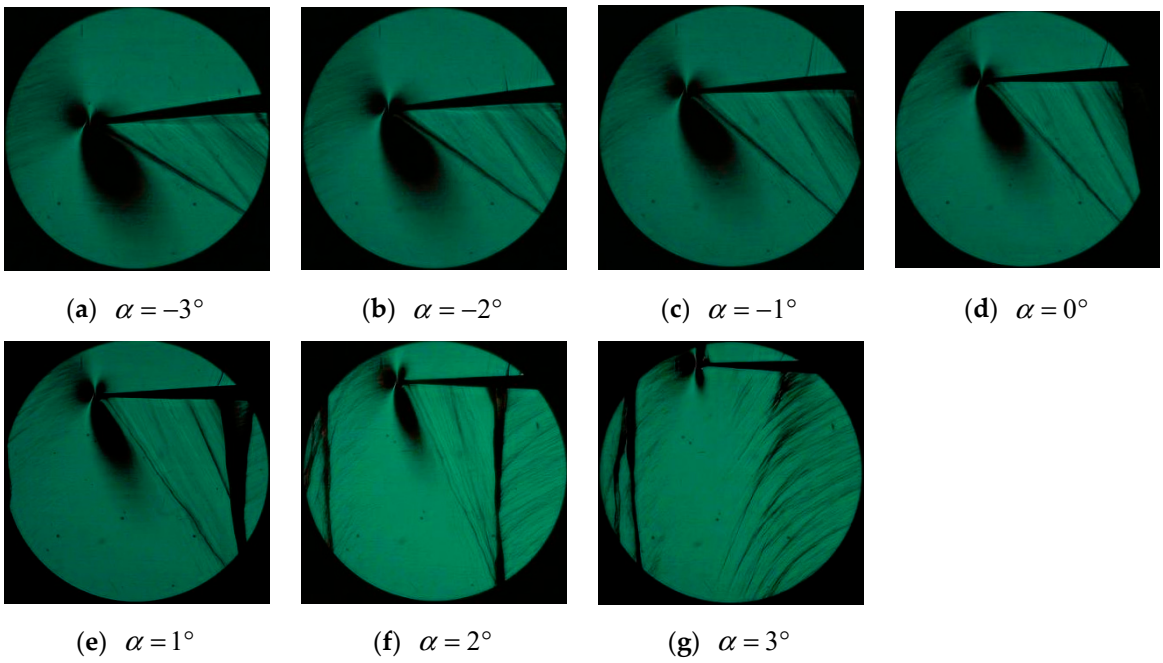

Figure 9. CM1.2-Y blade profile, Mach number 1.05 schlieren image.

Based on these results, it can be concluded that at a Mach number of 1.05, optimizing the blade profile with leading-edge curvature can effectively reduce the pressure non-uniformity and shock wave intensity near the leading edge.

3.2. Pulsating Pressure Characteristics on the Blade Surface

3.2.1. Ma = 0.8

This study aims to investigate the impact of angle of attack variations on the unsteady surface pressure of a baseline compressor blade profile under transonic conditions. The chordwise sound pressure level measurements conducted on the CM1.2 blade profile at Mach number 0.8 and angles of attack of −2°, 0°, and +2° are shown in Figure 10a. The results indicate that the peak pressure pulsation consistently occurs in the region near the leading edge on the suction surface (approximately near measurement point 11), with sound pressure levels ranging from 156 to 157 dB, and this peak position does not vary with changes in the angle of attack. Changes in the angle of attack primarily affect the amplitude of the pulsation: the peak sound pressure level is highest at $\alpha = 0°$ (approximately 156.8 dB), while at $\alpha = +2°$, the sound pressure level significantly increases in the mid-chord section (measurement points 3–7) on the suction surface. These results suggest that at Mach number 0.8, the primary unsteady excitation source of this blade profile is fixed in a specific region on the suction surface. The high-pulsation region does not vary with changes in the angle of attack, which clarifies the key geometric optimization objectives and their associated impact mechanisms.

To evaluate the enhancement effect of leading-edge curvature optimization on the adaptability to angles of attack, tests were conducted on the optimized CM1.2-Y airfoil under the same conditions, as shown in Figure 10b. At angles of attack of −2°, 0°, and +2°, the sound pressure level distribution was significantly suppressed within a lower range of 141–146 dB. Importantly, the characteristic peak of 156–157 dB near measurement point 11 of the baseline airfoil was completely eliminated. Therefore, the leading-edge curvature optimization achieved decisive success at a Mach number of 0.8. This optimization not only significantly reduced unsteady loads but also completely eliminated sensitivity to

angles of attack, enabling the airfoil to maintain a low pulsating flow state throughout the entire test range of the angles of attack from −2° to +2°.

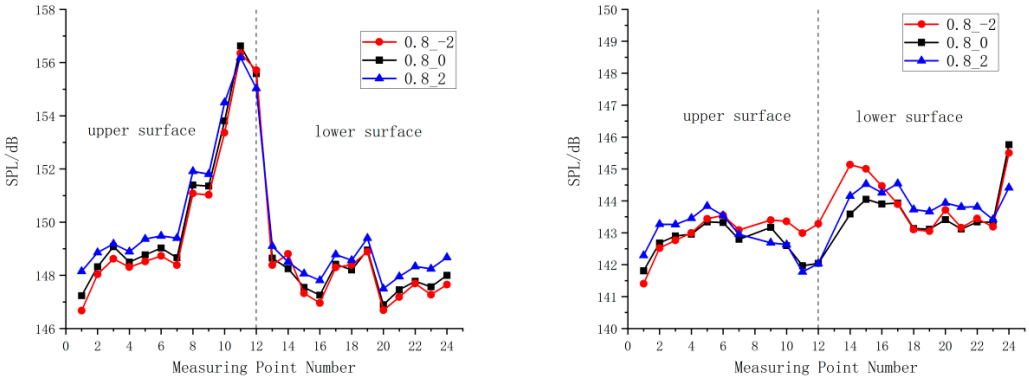

(**a**) CM1.2 (**b**) CM1.2-Y

Figure 10. Surface sound pressure level distribution of CM1.2 airfoil and CM1.2-Y airfoil at Mach number 0.8.

Figure 11 comprehensively compares the chordwise sound pressure level distribution of the baseline CM1.2 airfoil and the optimized CM1.2-Y airfoil at Mach number 0.8 and angles of attack of −2°, 0°, and +2°. The results indicate that the optimization brings comprehensive and significant improvements. The baseline airfoil consistently exhibits a sharp characteristic pressure pulsation peak near measuring point 11 on the suction surface, with sound pressure levels of 156.4 dB, 156.6 dB, and 156.2 dB at angles of attack of −2°, 0°, and +2°, respectively. The optimized design completely eliminates this local peak, achieving reductions of 13.4 dB, 14.6 dB, and 14.4 dB at the corresponding angles of attack, respectively. Therefore, the maximum sound pressure level on the suction surface of the optimized airfoil is reduced to approximately 141.8 dB at an angle of attack of +2°, and maintained at the same low level at other angles of attack. In addition, the pressure distribution across the entire airfoil surface becomes significantly more uniform and smoother. It can be concluded that at Mach number 0.8, the leading-edge curvature modification effectively suppresses shock waves and controls separation by reshaping the pressure distribution and eliminating the pressure peak on the suction surface leading edge, thereby significantly reducing unsteady pressure pulsations across the entire range of tested angles of attack.

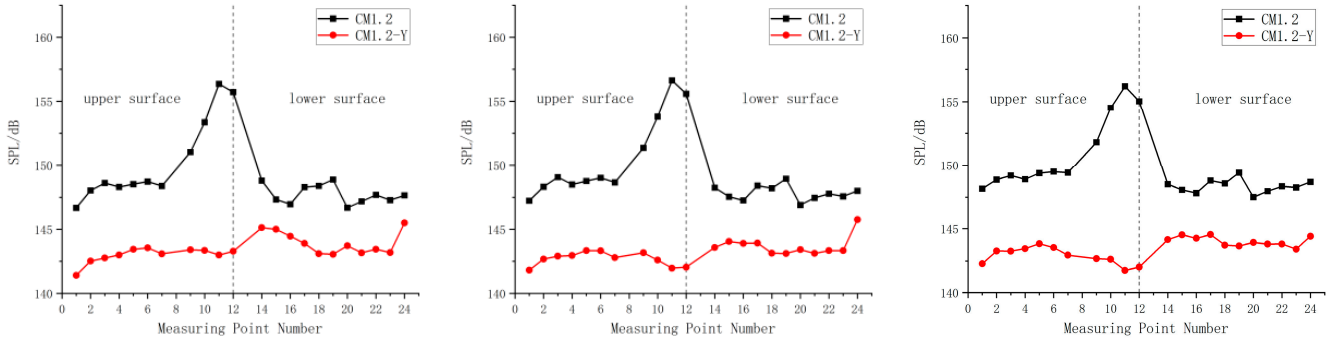

(**a**) $\alpha = -2°$ (**b**) $\alpha = 0°$ (**c**) $\alpha = 2°$

Figure 11. Comparison of sound pressure level on the surface of CM1.2 airfoil and CM1.2-Y airfoil at Mach number 0.8.

To further reveal the physical laws behind the optimization effect, the influence of leading-edge curvature optimization on flow unsteadiness was analyzed from the frequency

dimension. As shown in Figure 11, the optimization effects are similar at angles of attack of −2°, 0°, and +2°. Therefore, taking Mach number 0.8 and an angle of attack of 0° as an example, the frequency spectra of surface fluctuating pressure for the baseline airfoil CM1.2 and the optimized airfoil CM1.2-Y were compared, as illustrated in Figure 12. The results indicate that the optimization significantly improves the pressure fluctuation characteristics across all frequency bands. In the mid-frequency range (100 Hz to 1 kHz), the optimized airfoil completely eliminates the wide-frequency energy peaks with amplitudes exceeding 160 dB observed in the baseline airfoil, reducing the sound pressure level in this frequency band by 40–50 dB. In the high-frequency range (1 kHz to 10 kHz), the optimized airfoil attenuates the high energy peaks of 140–165 dB in the baseline airfoil by 60–70 dB, causing the spectrum to rapidly decay to 80–100 dB above 1 kHz. These results reveal that leading-edge curvature optimization effectively suppresses mid-frequency pulsations dominated by local shock wave oscillations and large-scale separations, and almost eliminates high-frequency noise originating from shock wave–boundary layer interactions and turbulence, thereby transforming the flow state on the airfoil surface from a strongly unsteady, shock wave-dominated mode to a more stable, milder attached flow mode.

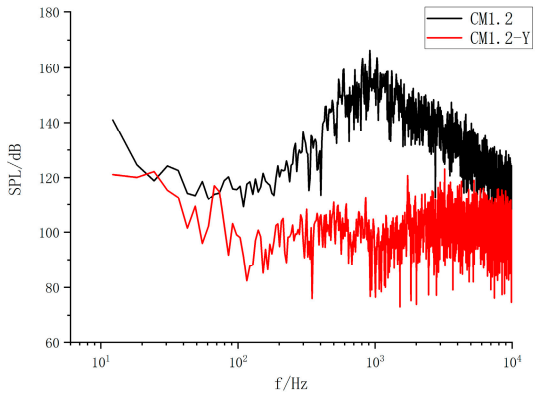

Figure 12. Comparison of sound pressure spectrum at 11 measuring points on the surface of CM1.2 and CM1.2-Y airfoils at Mach number 0.8 and angle of attack of 0°.

3.2.2. Ma = 0.95

The chordwise sound pressure level measurements conducted on the CM1.2 airfoil at a Mach number of 0.95 and angles of attack of −2°, 0°, and +2° are shown in Figure 13a. The results indicate that the fluctuating pressure distribution is highly sensitive to changes in the angle of attack and is asymmetric. At an angle of attack of −2°, a highly localized pressure peak appears at measuring point 13 on the pressure surface (lower surface leading edge), with a sound pressure level reaching 152.6 dB. This peak significantly exceeds the sound pressure level at other angles of attack. However, at angles of attack of 0° and +2°, the sound pressure level distribution is relatively smooth, without similar extreme peaks. From this, it can be concluded that the leading edge of the pressure surface (lower surface) of the baseline CM1.2 airfoil exhibits critical sensitivity to shock wave impact under negative angle of attack conditions at a Mach number of 0.95, which can induce highly localized extreme pressure fluctuations.

Subsequently, the influence of leading-edge curvature optimization on the unsteady pressure characteristics and its sensitivity to the angle of attack of the CM1.2-Y blade profile was evaluated under the same conditions, as detailed in Figure 13b. This optimization fundamentally altered the pulsation patterns and peak intensities. Significant localized peaks appeared on the suction side (leading edge of the upper surface): specifically, at an angle of attack of 2°, an extreme localized peak occurred at measuring point 3 on the upper surface, with a sound pressure level reaching 157.0 dB, higher than the maximum

pulsation of the baseline blade profile; at an angle of attack of 0°, an extreme localized peak appeared at measuring point 5, with a sound pressure level of 152.3 dB; and at an angle of attack of −2°, an extreme localized peak occurred, with a sound pressure level of 156.5 dB. Compared to the baseline blade profile, the sharp peaks at the leading edge of the lower surface disappeared at angles of attack of −2°, 0°, and 2°. Therefore, it can be concluded that leading-edge curvature optimization shifted the main sensitive area of pulsating pressure from the leading edge of the pressure surface (lower surface) under negative angles of attack to the suction surface (upper surface) across the entire range of tested angles of attack. Although it successfully eliminated the shock wave sensitive points on the pressure surface, under Mach number 0.95 conditions, this optimized design may lead to a more forward and concentrated position of the shock wave on the suction surface at positive angles of attack, inadvertently amplifying local unsteady loads.

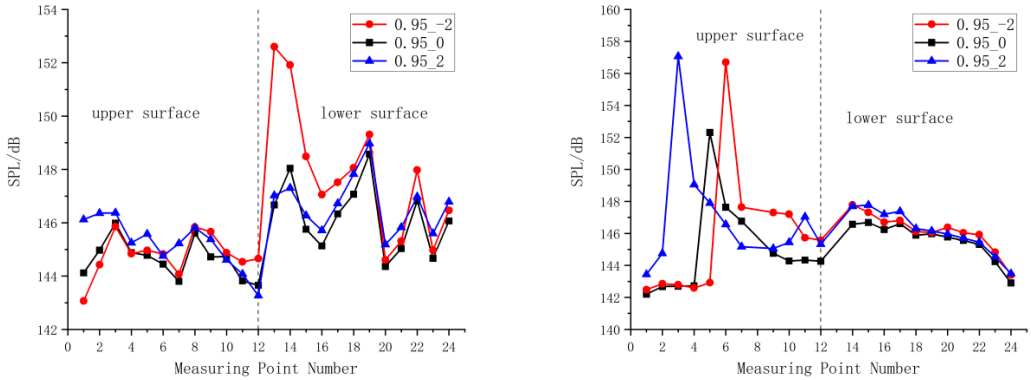

(**a**) CM1.2 (**b**) CM1.2-Y

Figure 13. Surface sound pressure level distribution of CM1.2 airfoil and CM1.2-Y airfoil at Mach number 0.95.

Figure 14 comprehensively compares the chordwise sound pressure level distributions of the baseline CM1.2 airfoil and the optimized CM1.2-Y airfoil at Mach number 0.95 and angles of attack of −2°, 0°, and +2°. The research results reveal a complex, condition-dependent trade-off relationship, as shown in Table 2. The optimization of leading-edge curvature brings benefits to the flow on the pressure surface (lower surface), effectively reducing or eliminating the characteristic pulsation peaks at measurement points 14, 19, and 22, and resulting in a more uniform pressure distribution. However, it simultaneously brings significant adverse effects to the suction surface (upper surface). Notable new pressure pulsation peaks appear on the suction surface (upper surface leading edge): the sound pressure level reaches 156.7 dB at measurement point 6 in Figure 14a, 152.3 dB at measurement point 5 in Figure 14b, and 157.1 dB at measurement point 3 in Figure 14c. These peaks represent sharp jumps of 11.9 dB, 7.5 dB, and 10.7 dB, respectively, compared to the levels of the baseline airfoil at corresponding locations. This effect is attributed to the adverse forward movement and enhancement of the shock wave on the suction surface caused by changes in the leading-edge curvature, which promotes strong shock–boundary layer interactions. Therefore, under the given near-sonic conditions, this optimization transfers the high unsteadiness region from the pressure surface to the suction surface and significantly intensifies its strength, resulting in negative effects. This is in direct contrast to its role in suppressing separation and weak shock waves under subsonic conditions. It can be inferred that although the continuous optimization of leading-edge curvature can effectively alleviate subsonic flow separation, it also significantly adjusts the position and intensity of the shock wave when approaching the sonic speed. This may lead to adverse shock wave advancement at high subsonic speeds, inadvertently

exacerbating local unsteady loads. This finding emphasizes that aerodynamic optimization strategies must coordinate shock wave management and geometric design across the entire operating range.

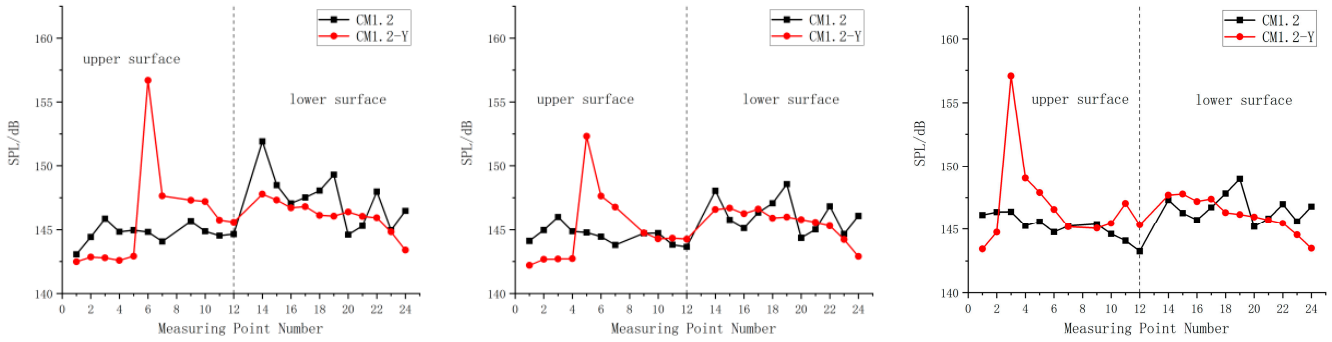

(**a**) $\alpha = -2°$ (**b**) $\alpha = 0°$ (**c**) $\alpha = 2°$

Figure 14. Comparison of sound pressure level on the surface of CM1.2 airfoil and CM1.2-Y airfoil at Mach number 0.95.

Table 2. Changes in sound pressure level after blade optimization at Mach number 0.95.

Measuring Point Number	Changes in Sound Pressure Level After Blade Optimiza-tion/dB ($\alpha = -2°$)	Changes in Sound Pressure Level After Blade Optimization/dB ($\alpha = 0°$)	Changes in Sound Pressure Level After Blade Optimi-zation/dB ($\alpha = 2°$)
3	−3.1	−3.3	10.7
5	−2.0	7.5	2.3
6	11.9	3.2	1.8
14	−4.1	−1.5	0.4
19	−3.3	−2.6	−2.8
22	−2.1	−1.5	−1.5

Similar to the Mach number 0.8 condition, to evaluate the spectral characteristics of leading edge curvature optimization under the Mach number 0.95 condition, the surface pressure fluctuation spectra of the baseline airfoil CM1.2 and the optimized airfoil CM1.2-Y were compared under the conditions of Mach number 0.95 and an angle of attack of −2°, as shown in Figure 15. The results indicate that the continuity of leading-edge curvature leads to more complex spectral variations. Although the average sound pressure level (SPL) of the optimized airfoil CM1.2-Y decreases compared to the baseline airfoil across the entire frequency band (10 Hz–10 kHz), its spectral shape transitions from a relatively smooth broadband characteristic to the appearance of spikes in the low-frequency range (10–100 Hz). Specifically, new significant spikes (SPL approximately 140 dB) appear in the low-frequency range (10–100 Hz); several peaks also appear in the mid-frequency range (100–1000 Hz); and in the high-frequency range (1000–10,000 Hz), despite an average energy attenuation of approximately 10–20 dB, instantaneous spikes higher than 120 dB still occur intermittently. These results suggest that under the Mach number 0.95 condition, although leading-edge curvature optimization reduces the overall energy of pressure fluctuations to some extent, it alters the unsteady characteristics of shock–boundary layer interactions, redistributes energy to lower frequencies, and may introduce new flow instabilities.

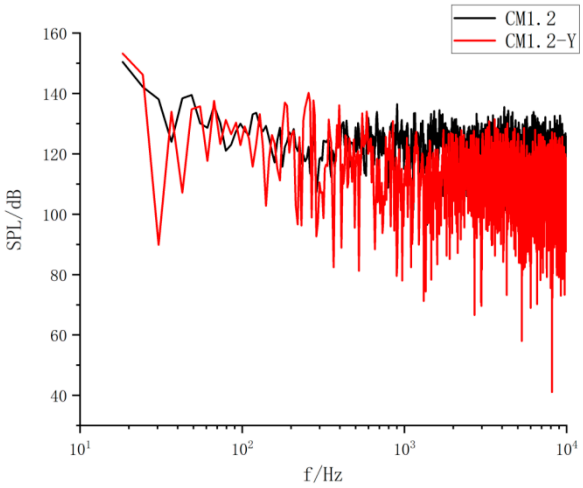

Figure 15. Comparison of sound pressure spectrum at 11 measuring points on the surface of CM1.2 and CM1.2-Y airfoils at Mach number 0.95 and angle of attack of −2°.

3.2.3. Ma = 1.05

The chordwise sound pressure level measurements of the CM1.2 airfoil at Mach 1.05 and angles of attack of −2°, 0°, and +2° are shown in Figure 16a. The results indicate that supersonic conditions induce significant pressure fluctuations: at an angle of attack of 2°, a sharp peak appears at measuring point 3 on the upper surface, with a sound pressure level reaching up to 160 dB, which is approximately 7.4 dB higher than the maximum fluctuation at Mach 0.95. From measuring point 3 to measuring point 4, the sound pressure level drops sharply from 160 dB to 148.8 dB, a decrease of 11.2 dB, indicating a highly concentrated source of fluctuations. The overall pressure level on the pressure surface (lower surface) is relatively low, with sound pressure levels generally ranging from 145 to 152 dB, with a local peak of approximately 152 dB at measuring point 19. At an angle of attack of −2°, a secondary peak of 158.6 dB appears at measuring point 7 on the upper surface. At an angle of attack of 0°, a peak of 151.4 dB appears at measuring point 5 on the upper surface. This indicates that at Mach 1.05, the location and amplitude of the dominant pressure fluctuation peak are highly dependent on the angle of attack, and the suction surface level consistently remains higher than the pressure surface, with large and concentrated pressure fluctuations. This suggests that the core mechanism generating extreme unsteady loads is the shock wave and its induced large-scale flow separation.

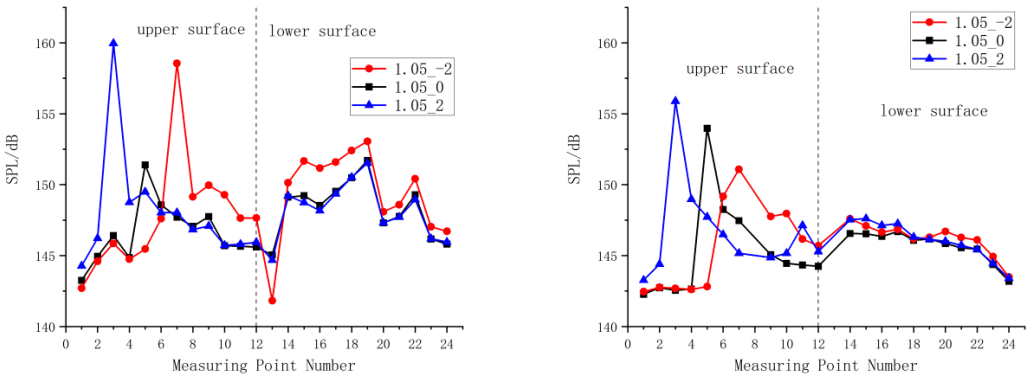

(**a**) CM1.2 (**b**) CM1.2-Y

Figure 16. Surface sound pressure level distribution of CM1.2 airfoil and CM1.2-Y airfoil at Mach number 1.05.

Subsequently, under the same conditions, the effectiveness of leading-edge curvature optimization on suppressing the aforementioned pulsations in the CM1.2-Y blade profile was evaluated, as shown in Figure 16b. The results indicate that leading-edge curvature optimization significantly reduces the level of pressure pulsations: for an attack angle of 2°, the peak sound pressure level at the leading edge of the suction surface decreases to 155.9 dB, a reduction of 4.1 dB relative to the baseline blade profile. For an attack angle of −2°, the peak value drops to 151.1 dB, representing a decrease of 7.5 dB. Furthermore, at all attack angles, the sound pressure level on the pressure surface decreases by approximately 7 dB overall, with a more uniform distribution. These findings confirm that leading-edge curvature optimization effectively suppresses shock–boundary layer interactions by adjusting the pressure distribution at the leading edge, successfully reducing the peak pulsation level on the suction surface and the overall unsteadiness on the pressure surface.

Figure 17 comprehensively compares the chordwise sound pressure level distribution of the baseline CM1.2 airfoil and the optimized CM1.2-Y airfoil at a Mach number of 1.05 and angles of attack of −2°, 0°, and +2°. As shown in Figure 17a, at an angle of attack of −2°, the continuous optimization of the leading-edge curvature has achieved clear success. On the suction surface (upper surface), the peak value of extreme pressure pulsation decreases from 158.6 dB at measurement point 7 of the baseline airfoil to 151.1 dB, a reduction of 7.5 dB, and the sound pressure levels at all suction surface measurement points have decreased. On the pressure surface (lower surface), the peak value of 153.1 dB at measurement point 19 of the baseline airfoil is completely eliminated. The maximum sound pressure level on the pressure surface is controlled within 148 dB, with an overall sound pressure level reduction ranging from 1.4 to 6.8 dB. This confirms that under supersonic negative angles of attack, optimization of the leading-edge curvature effectively reduces the extreme pulsations on the suction surface caused by shock wave interference and significantly improves the wave structure on the pressure surface, thereby comprehensively reducing the pressure pulsation level of the airfoil.

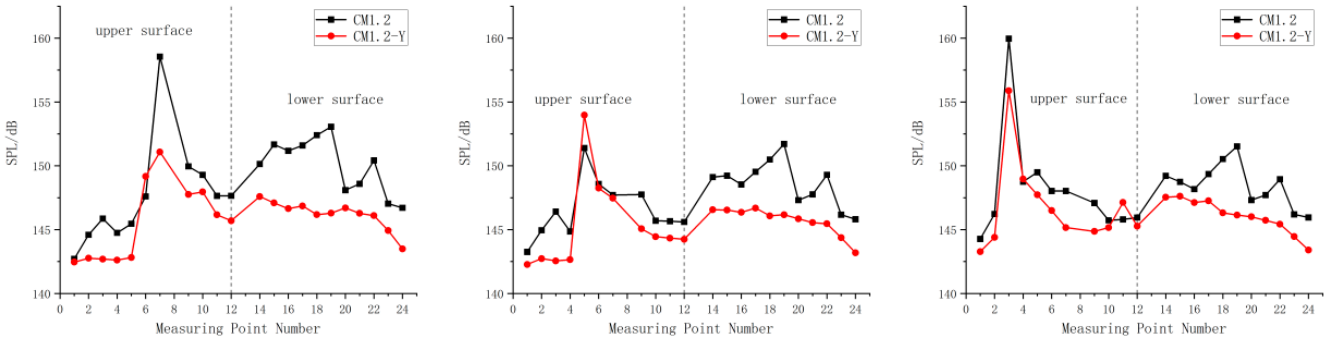

Figure 17. Comparison of sound pressure level on the surface of CM1.2 airfoil and CM1.2-Y airfoil at Mach number 1.05.

As shown in Figure 17b, at an angle of attack of 0°, both optimization effects and negative effects coexist. The optimized airfoil CM1.2-Y generally reduces the sound pressure level from measuring point 1 to 12 on the suction surface, except for measuring point 5, where a new peak is generated, resulting in an increase of 2.6 dB in sound pressure level. The maximum reduction on the suction surface is 3.9 dB at measuring point 3. However, comprehensive improvements have been achieved on the pressure surface, completely eliminating the characteristic peaks of the baseline airfoil at measuring points 19 and 22. The maximum sound pressure level on the pressure surface is controlled within 146.7 dB, corresponding to a maximum reduction of 5.5 dB. This indicates that the optimization

effectively contracts the high-pulsation region dominated by shock wave-boundary layer interaction on the suction surface and significantly stabilizes the flow on the pressure surface. However, the persistent high-amplitude peak at measuring point 5 on the suction surface suggests that additional local improvements may be necessary to achieve comprehensive optimization.

As shown in Figure 17c, at an attack angle of 2°, the optimized effect exhibits significant regional differences. On the suction surface, the extreme peak at measuring point 3 decreases from 160.0 dB for the baseline blade profile to approximately 155.9 dB for the optimized blade profile, a reduction of 4.1 dB. The sound pressure level (SPL) at downstream positions on the suction surface (measuring points 4–12) also decreases overall, with a maximum reduction of 2.9 dB. However, the pressure surface achieves comprehensive success. The optimization completely eliminates the 151.5 dB peak at measuring point 19 for the baseline blade profile and maintains the overall sound pressure level on the pressure surface at a stable low level of 143.4–147.6 dB, achieving a maximum reduction of 5.4 dB. These results indicate that under supersonic positive attack angles, leading edge curvature optimization has limited direct ability to mitigate extreme shock wave interference on the leading edge of the suction surface, but it is very effective in improving the wave structure on the pressure surface, thereby significantly enhancing the flow stability of the pressure surface.

To evaluate the spectral characteristics of leading-edge curvature optimization under Mach 1.05 conditions, the surface pressure fluctuation spectra of the baseline airfoil CM1.2 and the optimized airfoil CM1.2-Y were compared under Mach 1.05 and an angle of attack 0°, as shown in Figure 18. The sound pressure level of the optimized airfoil CM1.2-Y was significantly lower than that of the baseline airfoil across the entire frequency band (10 Hz–10 kHz). Specifically, in the mid-frequency range (100 Hz–1 kHz), its sound pressure level decreased by 10–20 dB; in the high-frequency range (1 kHz–10 kHz), the sound pressure level attenuation was more pronounced, decreasing by 20–60 dB, with energy in some frequency bands dropping to 60–80 dB. These results indicate that under Mach 1.05 and an angle of attack of 0°, the optimized model exhibits lower pressure fluctuation levels in most frequency ranges, and changes in leading-edge curvature have a significant impact on the pulsating pressure characteristics of the blade surface. Leading-edge curvature optimization can effectively suppress mid- and high-frequency pulsations dominated by small-scale turbulence but has limited improvement on low-frequency components dominated by macroscopic oscillations of shock waves.

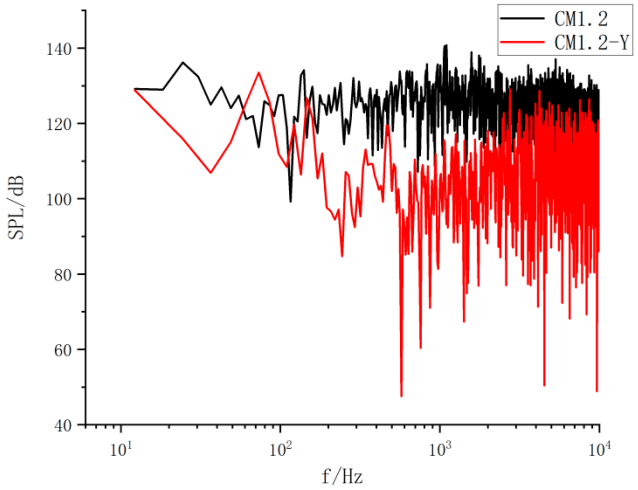

Figure 18. Comparison of sound pressure spectrum at 11 measuring points on the surface of CM1.2 and CM1.2-Y airfoils at Mach number 1.05 and angle of attack of 0°.

4. Conclusions

This study investigated the effect of leading-edge curvature optimization on the flow structure and unsteady pressure pulsation characteristics of transonic compressor blade profiles through schlieren and pulsating pressure tests. The main conclusions are as follows:

(1) At a Mach number of 0.8 and an angle of attack of -2° to 2°, the optimization of the leading-edge curvature comprehensively reduces the pulsating pressure level on the blade surface, significantly reducing the sound energy near the frequency of 1000 Hz. The maximum sound pressure level drop at a single measurement point reaches 14.6 dB.

(2) At a Mach number of 0.95 and an angle of attack of -2° to 2°, the optimization of the leading-edge curvature reduces the pulsating pressure level on the pressure surface, with a maximum decrease of 4.1 dB. However, a new peak pressure pulsation appears on the suction surface, with a maximum increase of 11.9 dB.

(3) At a Mach number of 1.05 and an angle of attack of -2° to 2°, the optimization of the leading-edge curvature almost completely reduced the pulsating pressure level on the blade surface, significantly reducing the sound energy near the frequency of 1000 Hz. The maximum sound pressure level drop at a single measurement point reached 7.5 dB.

(4) The optimization of leading-edge curvature has a significant effect on reducing the level of pulsating pressure on the blade surface, but on the other hand, it also reflects the high sensitivity and potential working condition dependence of the optimization effect on the incoming Mach number. Future research can delve into how the geometry of the leading edge affects the physical mechanism of pressure pulsation in different frequency bands by finely regulating the position and shape of shock waves, and develop intelligent and adaptive leading-edge design methods that can coordinate sub/cross/supersonic multi-condition targets.

Author Contributions: Conceptualization, Y.Y. (Ye Yang) and J.W.; methodology, Y.Y. (Ye Yang) and S.H.; software, Y.Y. (Ye Yang); validation, Y.Y. (Ye Yang), Y.Y. (Yuan Yi) and X.D.; formal analysis, Y.Y. (Ye Yang); investigation, Y.Y. (Ye Yang) and S.H.; resources, J.W.; data curation, Y.Y. (Ye Yang) and Y.Y. (Yuan Yi); writing—original draft preparation, Y.Y. (Ye Yang); writing—review and editing, J.W.; visualization, Y.Y. (Ye Yang); supervision, Y.Y. (Yuan Yi); project administration, X.D.; funding acquisition, J.W. All authors have read and agreed to the published version of the manuscript.

Funding: This research received no external funding.

Institutional Review Board Statement: Not applicable.

Informed Consent Statement: Not applicable.

Data Availability Statement: Data available on request due to privacy.

Conflicts of Interest: The authors declare no conflicts of interest.

References

1. Lee, B.H.K. Transonic buffet on a supercritical aerofoil. *Aeronaut. J.* **1990**, *94*, 143–152. [CrossRef]
2. Hergt, A.; Klinner, J.; Grund, S.; Willert, C.E. Experimental investigation of shock-induced separation and flow control in a transonic compressor cascade. *Exp. Fluids* **2019**, *60*, 96. [CrossRef]
3. Klinner, J.; Hergt, A.; Grund, S.; Willert, C.E. High-speed PIV of shock boundary layer interactions in the transonic buffet flow of a compressor cascade. *Exp. Fluids* **2021**, *62*, 58. [CrossRef]
4. Hah, C. Large eddy simulation of transonic flow field in NASA Rotor 37. In Proceedings of the 47th AIAA Aerospace Sciences Meeting Including the New Horizons Forum and Aerospace Exposition, Orlando, FL, USA, 5–8 January 2009.
5. Denton, J.D. Multall—An open source, computational fluid dynamics based, turbomachinery design system. *J. Turbomach.* **2017**, *139*, 121001. [CrossRef]
6. Meng, F.; Gong, C.; Li, K.; Xiong, J.; Li, J.; Guo, P. Aerodynamic optimization and mechanism investigation on performance improvements in a transonic compressor cascade. *Machines* **2023**, *11*, 244. [CrossRef]

7. Zou, L.; Lv, C.; Gui, L.; Wang, W.; Huang, Y. Collaborative improvement of profile accuracy and aerodynamic performance in robotic grinding of transonic compressor blade leading edge. *Aerosp. Sci. Technol.* **2024**, *146*, 108937. [CrossRef]
8. Li, H.; Zou, L.; Wang, W.; Gui, L. Redesign and machining of leading edge of transonic compressor blade in robotic grinding operation. In *Proceedings of the 33rd International Council of the Aeronautical Sciences (ICAS 2024)*; ICAS: Ultimo, NSW, Australia, 2024.
9. Denton, J.D. Loss mechanisms in turbomachines. *J. Turbomach.* **1993**, *115*, 621–656. [CrossRef]
10. Hilgenfeld, L.; Fottner, L. Experimental investigation of turbulence structures in a highly loaded transonic compressor cascade with shock/laminar boundary layer interactions. In *Engineering Turbulence Modelling and Experiments 5*; Elsevier Science Ltd.: Oxford, UK, 2002; Volume 5, pp. 779–788. [CrossRef]
11. Du, W.H.; Wu, H.; Ruan, J.G. A shock loss model for the transonic axial compressor. *J. Aerosp. Power* **2007**, *22*, 922–928. (In Chinese)
12. Yang, H.; He, L. Experimental study on linear compressor cascade with three-dimensional blade oscillation. *J. Propuls. Power* **2004**, *20*, 180–188. [CrossRef]
13. Goodhand, M.N.; Miller, R.J. Compressor leading edge spikes: A new performance criterion. *J. Turbomach.* **2011**, *133*, 021006. [CrossRef]
14. Shi, H.T.; Liu, B.J.; Yu, X.J. A curvature continuous leading edge modeling method based on polynomial and its application. *J. Aerosp. Power* **2020**, *35*, 397–409. (In Chinese) [CrossRef]
15. Khan, A.; Ullah, T.; Ahmad, F.; Siddiqi, M.U.R.; Hanif, M.I.; Irfan, M.; Ali, S. Blade Meridional Profile Optimization for Novel High-Pressure Ratio Centrifugal Compressor Design Using Numerical Simulations. In *Proceedings of the 2020 3rd International Conference on Computing, Mathematics and Engineering Technologies (iCoMET), Sukkur, Pakistan, 29–30 January 2020*; IEEE: New York, NY, USA, 2020; pp. 1–9.
16. Wu, D.; Xu, C.; Yang, Y. Leading edge optimization design of transonic airfoil for axial flow compressor. *J. Ordnance Equip. Eng.* **2023**, *44*, 246–253. (In Chinese) [CrossRef]
17. Chen, H.; Gao, C.; Wu, J.; Ren, K.; Zhang, W. Study on optimization design of airfoil transonic buffet with reinforcement learning method. *Aerospace* **2023**, *10*, 486. [CrossRef]
18. Wang, W.; Feng, H.; Cui, S.; Li, Z. Multi-objective optimization of transonic variable camber airfoil with leading- and trailing-edge deflections using Kriging surrogate model. *Aerospace* **2025**, *12*, 659. [CrossRef]
19. Liu, Y.; Chen, J.; Cheng, J.; Xiang, H. Aerodynamic optimization of transonic rotor using radial basis function based deformation and data-driven differential evolution optimizer. *Aerospace* **2022**, *9*, 508. [CrossRef]
20. Giannelis, N.F.; Vio, G.A.; Levinski, O. A review of recent developments in the understanding of transonic shock buffet. *Prog. Aerosp. Sci.* **2017**, *92*, 39–84. [CrossRef]
21. Munoz Lopez, E.J.; Hergt, A.; Grund, S.; Gümmer, V. The unsteady shock-boundary layer interaction in a compressor cascade—Part III: Mechanisms of shock oscillation. *J. Turbomach.* **2024**, *146*, 081001. [CrossRef]
22. Meng, F.; Tang, J.; Li, J.; Zhong, J.; Guo, P. Large eddy simulation of shock wave/boundary layer interactions in a transonic compressor cascade. *Phys. Fluids.* **2024**, *36*, 076121. [CrossRef]
23. Meng, F.; Li, K.; Guo, P.; Gan, J.; Li, J. Experimental and numerical investigations of shock-wave boundary layer interactions in a highly loaded transonic compressor cascade. *J. Therm. Sci.* **2024**, *33*, 123–135. [CrossRef]
24. Watanabe, T.; Azuma, T.; Uzawa, S.; Himeno, T.; Inoue, C. Unsteady pressure measurement on oscillating blade in transonic flow using fast-response pressure-sensitive paint. *J. Turbomach.* **2018**, *140*, 061003. [CrossRef]
25. Malzacher, L.; Schwarze, C.; Motta, V.; Peitsch, D. Experimental investigation of an aerodynamically mistuned oscillating compressor cascade. *J. Turbomach.* **2019**, *141*, 071012. [CrossRef]
26. Gan, J.; Watanabe, T.; Himeno, T. Effect of shock wave behavior on unsteady aerodynamic characteristics of oscillating transonic compressor cascade. *J. Eng. Gas Turbines Power* **2022**, *144*, 021025. [CrossRef]
27. *GJB 1179-1991*; Specification for Flow Quality of High and Low Speed Wind Tunnels. Commission of Science, Technology and Industry for National Defense: Beijing, China, 1991.
28. Kulfan, B.M.; Bussoletti, J.E. Fundamental Parametric Geometry Representations for Aircraft Component Shapes. In Proceedings of the 11th AIAA/ISSMO Multidisciplinary Analysis and Optimization Conference, Portsmouth, VA, USA, 6–8 September 2006.